CORROSION SCIENCE AND TECHNOLOGY, Vol.23, No.1(2024), pp.11~19 pISSN 1598-6462 / eISSN 2288-6524
[Research Paper] DOI: https://doi.org/10.14773/cst.2024.23.1.11

Corrosion Behavior of Fe-Ni Bainitic Steel Through an Inverted Austempering Multi-Step Process for Weathering Steel Applications

Miftakhur Rohmah[1,†], Gusti Umindya Nur Tajalla[2], Gilang Ramadhan[2], Yunita Triana[2], and Efendi Mabruri[1]

[1]*Research Center for Metallurgy, National Research and Innovation Agency (BRIN), South Tangerang, 15314, Indonesia*
[2]*Department of Materials and Metallurgical Engineering, Institut Teknologi Kalimantan, Balikpapan, 76127, Indonesia*
(Received February 07, 2023; Revised June 06, 2023; Accepted June 07, 2023)

A Fe-Ni Bainitic steel as a weathering steel application was developed by combining its excellent mechanical properties and corrosion resistance in maritime environments. Nickel concentration (0.4-3 wt%) and inverted austempering multi-step (IAM) process were primary determinants of the microstructure of the Fe-Ni Bainitic steel. The initial austempering steel was performed at 300 °C for 600 seconds to obtain a partly bainitic transformation. The steel was heated again for 1800 s at 450 °C. The microstructure was comprised of ferrite, a blocky martensite/austenite island, and a homogeneous lath-shape bainite structure with widths ranging from 4.67 to 6.89 μm. The maximum strength, 1480 MPa, was obtained with 3 wt% nickel. In this study, corrosion behavior was investigated utilizing potentiodynamic and electrochemical impedance spectroscopy (EIS) tests. A higher nickel content in Fe-Ni Bainitic steel refined the grain size, improved the bainite fraction, lowered the corrosion rate to 0.0257 mmpy, and increased the charge transfer of film resistance to 1369 Ω.

Keywords: *Inverted austempering multi-step process, Marine environment, Fe-Ni steel, Weathering steel*

1. Introduction

Steel properties, low cost-manufacturing techniques, design, and inspection contribute to the structure's reliability. Weathering steel (WS) is becoming more popular in outdoor structural materials due to its resistance to aggressive atmospheric corrosion. WSs often referred to known as high strength low alloy (HSLA), are designed to produce a compact oxide layer or "Patina" by regulating the composition and the repeated wetting-drying cycles [1]. Conventional WS contain 0.2 wt% carbon and 3-5 wt% total of Cu, P, Cr, Ni, Mn, Si, or other micro-alloy elements [2]. Among all the compositions, nickel is crucial to preventing embrittlement during the hot rolling process. Nickel disperses $NiFe_2O_4$ rust, hastening the formation of the α-FeOOH and inhibiting the Cl- entry into the oxide layer. A previous study found that increasing the nickel content by up to ~3 wt% improved corrosion resistance in marine [3] and acidic atmospheric environments [4] by lowering metallic ion hydrolysis. Adding more than 3.5 wt% Ni has a negligible impact and was not recommended to WS due to the high cost of production [5]. Another factor to consider is that the Ni/Cu ratio composition in WS must be considerably higher.

The refined bainitic matrix formation from heat treatment process is expected to improve corrosion-resistance WS [2,6,7]. The polarization corrosion behavior is depended on the existing phase and their fraction, chemical composition, and heat treatment. Neetu *et al*. [8] confirmed that the corrosion rate increases as the bainite fraction increase due to the micro-galvanic tendency. Granular bainite, on the other hand, corrodes more slowly than acicular ferrite during cyclic corrosion, according to Xiao *et al*. [9], The WS steel with bainite + polygonal ferrite produced of two parts of rust: the loose outer rust and the compact inner layer [7]. Based on the literature, the corrosion trend of bainitic steel is quite inconsistent-distinguished in corrosion, so advanced research is required to comprehend the precise mechanism of corrosion.

Microstructure and grain refinement are primary determinants of corrosion behavior and mechanical

†Corresponding author: miftakhur.rohmah@brin.go.id

properties. The strength level of commercial WS is only 400-550 MPa [10], which needs to be improved. A polyphase microstructure: austenite film layered among softer bainitic ferrite, produced by multi-step austempering (MAB) process, results in high tensile (up to 1428 MPa), better elongation (11-16%), and high impact strength [11]. Inverted austempering multi-step (IAM) can shorten the isothermal time by starting with a lower temperature step (~260 °C) for the first austempering and gradually increasing to a higher temperature (~360 °C) [12]. During this process, the massive austenite blocks broke up and became bainite, increasing mechanical stability.

Tensile and polarization test are used in this study to investigate the effect of Ni and bainite structure on the mechanical properties and corrosion behavior. It is crucial to develop high-quality steel for marine use.

2. Experimental Methods

The experimental steels' primary alloyed composition (in wt%) is 0.17C - 0.02Al – 0.49 Cr – 1.08 Mn – 0.4 Ni – 0.32 Cu – 0.43 Si – 0.064 V – 0.014 P - Fe (in wt%) (Bal). A varied nickel content of 1-3 wt% was added to main composition during melting process. The ingot was hot rolled to a 50% reduction (1 mm of thickness) and then air cooled after three hours of homogenization at 1100 °C. The continuous cooling transformation (CCT) curves of the tested steel as calculated by Jmatpro simulation are shown in Fig. 1a. The Bainite start (Bs) temperature of Fe-Ni Steel is 553 °C for 0.4 wt% Ni and 523 °C for 3 wt% Ni. Meanwhile, the Martensite start (Ms) temperature is 398 °C and 355 °C, respectively. Each specimen, measuring 100 × 10 × 5 mm, was cut from the rolled state and subjected to the inverted MAB procedure depicted in Fig. 1b. The sample was cooled to austempering temperature after 30 minutes of austenitization at 850 °C. In general, the first austempering steel was performed at 300 °C for 600 s to achieve a partially bainitic transformation. Then, the samples were heated again at 450 °C for 1800 s.

Following that, all specimens were analyzed. A 10 × 10 mm specimen was prepared to characterize the microstructure using a scanning electron microscope. The specimen was ground to 1500 grit with SiC paper, polished with 1μm alumina slurry, and etched with nital 2% + sodium metabisulfite10%. A tensile test was carried out on the Tinius Olsen Universal Testing Machine to evaluate the mechanical properties. The sub-size specimen test was prepared in 25 mm of gauge length and 6 mm of width in accordance with ASTM E8M specifications.

The electrochemical performance in NaCl solution was investigated using a Gamry workstation. Three electrodes were set following the purpose: platinum wire served as the counter electrode, a saturated calomel electrode served as a reference, and the 10 × 10 mm^2 exposed area sample served as the working electrode. Polarization and electrochemical impedance spectroscopy (EIS) were performed after wet/dry cyclic methods to assess the long-term corrosion resistance.

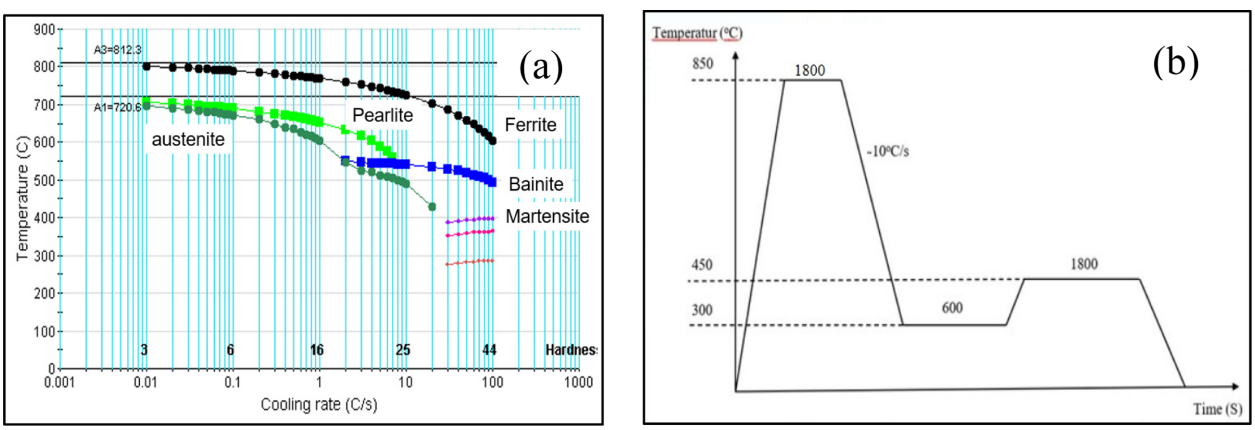

Fig. 1. (a) CCT simulation of tested steel and (b) schematic diagram of Inverted Multi-Step Austempering (MAB) Process

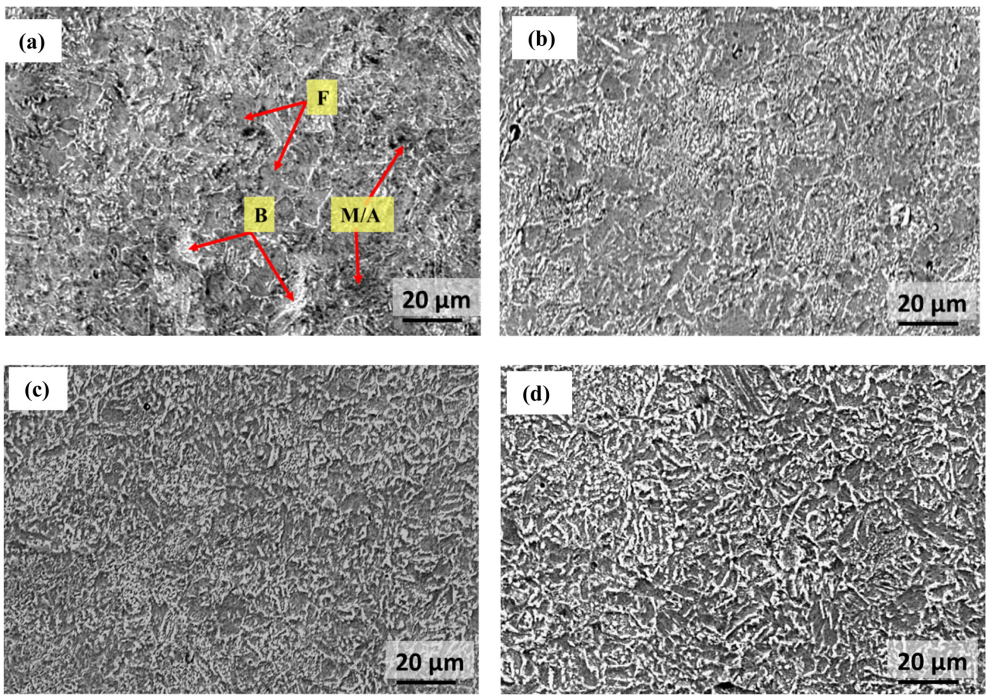

Fig. 2. SEM image of Fe-Ni (a) without nickel addition and with (b) 1 wt%, (c) 2 wt% and (d) 3 wt% nickel

3. Results and Discussion

3.1 Microstructure Analysis

The bainite formation using inverted multi-step austempering process in Fe-Ni steel is explained in CCT Diagram (Fig. 1a). Nickel addition shifted the CCT of ferrite and retained austenite transformation to the right. Carbon, nickel, and manganese are known to act as austenite stabilizing and enlarging the austenite phase region and shifting down the critical temperature of A_3 – Bs, and thereby, reducing the amount of bainite transformation [13]. In Fe-Ni steel with low carbon content, the bainite start temperature was successfully attained at a low temperature.

Fig. 2. shows the final microstructure of Fe-Ni steel after it underwent an inverted multi-step austempering process. It is composed of a lath-shape bainite structure (B mark) with denser-uniform distribution, ferrite (F mark), and blocky martensite/retained austenite island (M/A mark with light color). The carbon enriched of austenite ad the growth of displacive system occur simultaneously with the bainite formation [14]. During the initial austempering at lower temperature of 300 °C, the carbon in austenite increases and partially transforms to coarse bainite while the other becomes martensite, generating a M/A island [12]. The M/A could have resulted from carbon ejected of more bainite into undecomposed austenite and the metastable RA transformation between the bainite lath caused by external stress [14-16]. Because of the presence of nucleation site at the martensite-austenite interfaces, the kinetics of isothermal bainitic transition were faster at lower temperature austempering (slightly close to the Ms) than at higher temperature [17]. For 1, 2, and 3 wt% Ni addition, the average width of the M/A phase is 0.91 µm, 1.02 µm and 1.34 µm, respectively. Simultaneously, the width of lath bainite is ranges from 4.67 to 6.89 µm. By increasing the nickel content in Fe-Ni steel, the width of lath bainite narrows and grain size refines, which factors in improving yield strength and hardness [18] and indirectly influencing the corrosion process.

However, the nickel addition has no effect on the bainite morphology in all samples. Furthermore, the total volume fraction of bainite was 35.59%, 39.03%, 40.68% and 40.98% for 0.41, 1, 2, and 3 wt% nickel, as determined by ImageJ. The current findings are similar to those of Citrawati *et al.* [18], the volume fraction of bainite increases as the nickel concentration increases with a

single austempering process in a similar composition (Fe-0.3C-1.4Si-Ni). In their observations, the exceeded Ni prolongs austenite stability and suppresses ferrite transformation during slow cooling rate. Compared to single austempering, the polygonal M/A remains stable with decreasing size of 0.91 μm, as calculated by linear interception methods [12]. Ni addition does not promote bainite transformation alone; instead, it is caused by the austenite stabilization. The amount of bainite improved slightly as a result of the nickel addition, which provided more austenite for bainitic-ferritic transformation site, directly hindered the ferritic transformation, reduced the driving force for transformation, and decreased free energy between γ-α at higher temperatures of austempering [13,16].

3.2 Mechanical Properties

Fig. 3 depicts the tensile properties of Fe-Ni steel after the inverted multi-step austempering process. With the addition of nickel, the yield and tensile strength increases to 684 and 1480 MPa, respectively, without sacrificing ductility. The inverted multi-step austempering process is approved for providing high-strength in low-carbon bainitic steels, indicating the inhibition of dislocation movement due to carbide distribution within bainitic ferrite. In addition, the presence of 1 wt% Mn and 0.49 wt% Cr improved the steel strength through solid solution strengthening [19]. The result's increasing trend is similar to Yao *et al*. [13], demonstrating that more nickel leads to more grain boundary, grain refining strengthening, and the presence of M/A with high stability at room temperature.

Along with the higher tensile, Ni-added steel up to 2 wt% showed a slight decrease in elongation (around 18.3%), and significant losses to 15% when 3 wt% Ni added, confirming the presence of M/A phase. Furthermore, the product of tensile strength (TS) and total elongation (TE) increased with the nickel content from 15.41 to 22.20 GPa.% (TS × TE). The enhanced mechanical properties contribute from a synergistic effect of the nickel addition, bainite fraction volume increase, and grain size reduction. The bainitic growth begins by deforming parent austenite with no atom diffusion, which can lead to plastic deformation, and the dislocated accumulation, known as displacive mechanism [20]. Additionally, due to the lower carbon levels in undecomposed austenite, the blocky of M/A is brittle and considered unstable [16]. The current study's elongation is greater than the results of Gao *et al*. [12] and Arribas *et al*. [19], which used the quench-partitioning process in terms of bainite formation and was accompanied by a high nickel content in the investigated steel.

3.3 Corrosion Properties

Effect of nickel content on the corrosion behavior is presented in the Fig. 4 and Fig. 5, which obtained using polarization and EIS method in 3.5 vol.% NaCl solution. The polarization curves were fitted utilizing linear extrapolation, while the EIS spectra were analyzed using

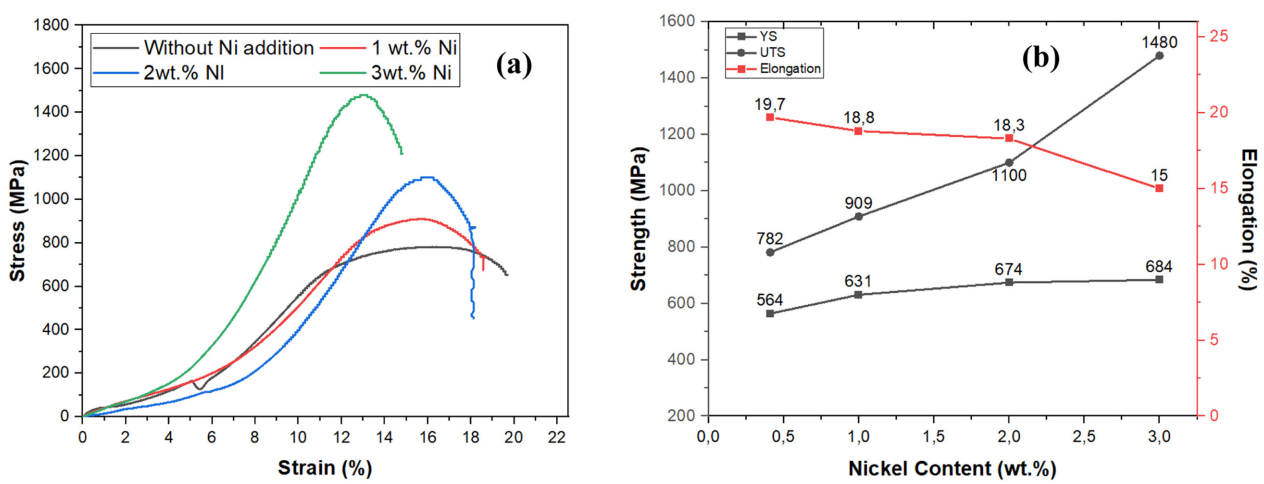

Fig. 3. Effect of nickel on the (a) stress-strain curve and (b) tensile properties of Fe-Ni Steels after the inverted multi-step austempering process

the equivalent electrical circuit (EEC), resulting in Table 1 and 2, respectively. Table 1 describes the corrosion parameters from polarization test, which includes of corrosion current density (I_{corr}), corrosion potential (E_{corr}), and corrosion rate. The cathodic reaction is estimated to be oxygen reduction ($O_2 + 2H_2O + 4e^- \rightarrow 4OH^-$), whereas the anodic reaction is the steel dissolution.

As shown in Fig. 4 and Table 1, adding nickel to Fe-Ni steel causes the corrosion potential to shift towards a more positive direction (from -789.4 mV to -575.0 mV) and the current density to move to left (reduced from 5.83 μA/cm^2 to 1.117 μA/cm^2), which implies a slower of corrosion rate. It also observed the metastable passivation in the sample with 0.41 wt% Ni content (without nickel addition), indicating the formation of a uniform-protective oxide layer as Cr-oxides, Fe-oxides, Ni-oxides or hydroxides [20,21]. Futhermore, the silicon content significantly improved the corrosion resistance in this steel after wet/dry cyclic process [22]. In chloride solution, the oxide layer of bainitic steel typically consist of β-FeOOH, γ-FeOOH, γ-Fe_2O_3, and Fe_3O_4, which can protect from further aggressive corrosion [21-23]. When subjected to micro-galvanic corrosion, a relatively smaller volume fraction bainite and rough structure experienced severe selective dissolution, resulting in a higher corrosion rate of 0.1567 mm/year. Moreover, as increasing the nickel content in Fe-Ni steels, the grain size refines, the bainite fraction improves and the corrosion rate slows to 0.02 mm/year, generating in a more stable of oxide layer. When compared to the 2% Ni sample, the corrosion value slighty increased with more nickel due to the increased bainite width and martensite fraction, in relation with Kazum *et al*. [24] and Song *et al*. [25]. However, the present study's corrosion rate more higher than Moon *et al.*'s [20] results due to the possibility of galvanic corrosion between bainite, M/A, and ferrite phases. Furthermore, by austempering at 400 °C, the refined bainite with finer carbide formation can significantly inhibit the corrosion rate. Because of its higher C content and increased energy reactivity, the bainite-ferrite phase is highly active corrosion than M/A phase. Hence, the higher bainite fraction is more resistant to corrosion [21].

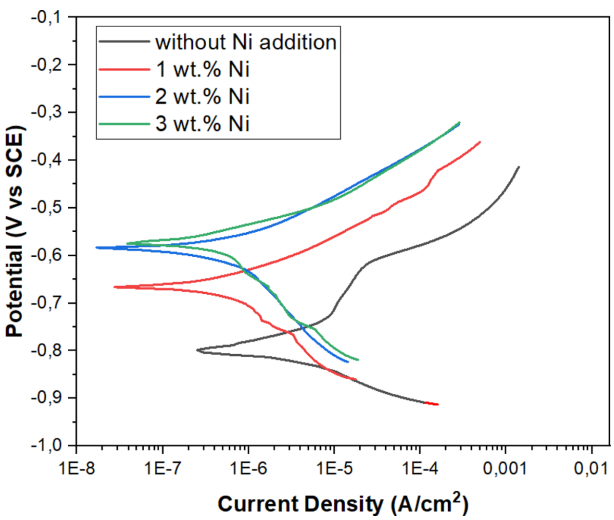

Fig. 4. Polarization curve of Fe-Ni steel in 3.5 vol.% NaCl solution

The EIS test was used to determine the specific of corrosion mechanism in each sample, which included the charge (ions/electron) transfer on the metal interface and the growth of an corrosion product. The EIS curve evolved similarly for all samples. As shown in Fig. 5d, a standard EEC (Rs(Qedl Rct // Qf Rf)) consist of electrolyte resistance (Rs), double layer capacitance (Qdl), charge-transfer resistance (Rt), film resistance correspond to layer oxide (Rf), film capacitance (Qf) (Table 2), indicating the

Table 1. Corrosion parameter of Fe-Ni steel

Sample	Polarization Test			Ref
	Ecorr (mV vs SCE)	Icorr (10^{-6} A/cm^2)	Corrosion rate (mm/year)	
Without Ni addition	-789.4	0.583	0.16	*
1 wt% Ni	-666.4	0.213	0.06	*
2 wt% Ni	-578.8	0.062	0.02	*
3 wt% Ni	-575.0	0.112	0.03	*
MS2 steel[a]	-713.1 to -477.5	0.05 to 25.2	0.001 to 0.28	[20]

*Present study, [a]0.47C-0.87Mn-0.51Si-0.15Cr-Fe(bal)(wt%)

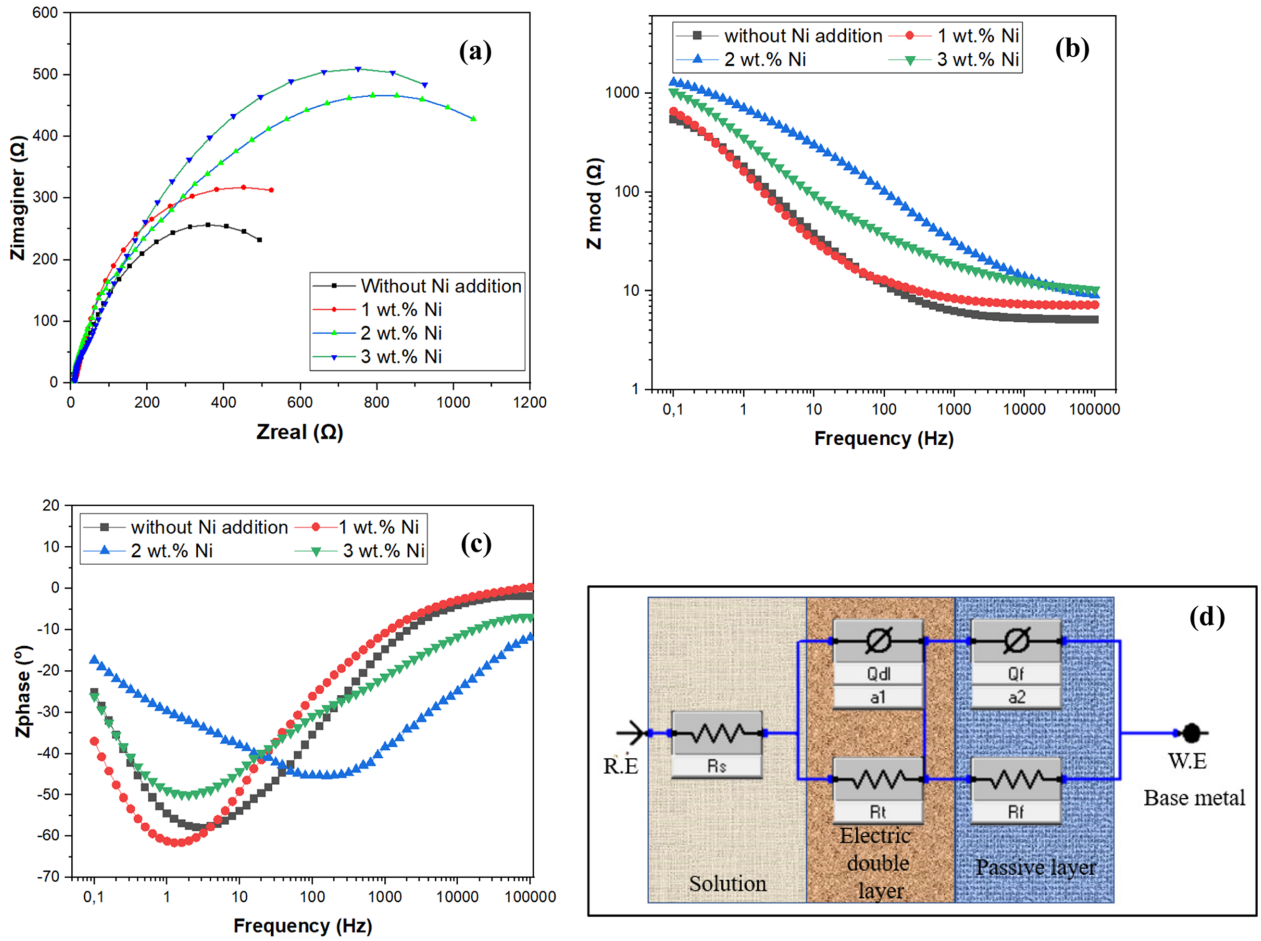

Fig. 5. EIS (a) Nyquist, (b) Bode Modulus, (c) Bode Phase plot, and (d) Equivalent electrical circuit

rust layer formation in the NaCl solution. This model is comparable to Barroux *et al*. [26]. Furthermore, in this study, a Chi-square (χ^2) value of 10^{-3} order (low error percentage) was considered for the best fitting of the EIS parameters.

Nyquist Plot in the Fig. 5a (|Zreal| vs. |Zimag| curve) demonstrates that the capacitive-incomplete semicircle at high frequency region plot has varying arc radius and width, indicating a rise in transfer resistance (Rt) as nickel addition increased, except for 1%Ni addition. The high diameter of the EIS spectra confirmed that the corrosion products have an excellent protective ability, which correlates with the potentiodynamic result (Fig. 4). Consequently, the ideal corrosion resistance is obtained by adding 2-3 wt% nickel with a high fraction of bainite (above 40%). The charge transfer the film resistance become 96.24 Ω and 1369 Ω. A higher Rct would result from in a lower corrosion rate (0.0177 mm/year for 2 wt% Ni and 0.0257 mm/year for 3 wt% Ni) and vice versa [27]. The corrosion dissolution reaction and the phenomenon of inhibition, which is indirecly related to the adsorption and desorption of rust layer, occurs in the low and intermediate frequency region in the 2% and 3% Ni (Fig. 5b and Fig. 5c). All sample's phase angles show maxima at high frequency regions and decrease with increasing nickel content (close 0° to -10°).

Table 2 shows the Rf value of 2 wt% Ni is 4 times higher (~1929 Ω) than the raw materials (523 Ω), confirming the better barrier function in the terms of the dense structure of the rust layer, which prevents the penetration of chloride ions and reduces the corrosion rate 274% to 0.0572 mmpy. According to the Bode plot (Fig. 5b-c), the solution resistance (Rs) is dominant at high frequency. On the other hand, low frequencies are dominated by total rust layer resistance (Rf) and interface of charge transfer resistance (Rt). As increasing the nickel

Table 2. EIS Parameter

Parameter	Sample			
	Without Ni addition	1 wt% Ni	2 wt% Ni	3 wt% Ni
Rs (Ω)	4.99 ± 0.06	7.04 ± 0.10	7.24 ± 0.16	8.74 ± 0.31
Qdl (µS*sâ)	1763 ± 299.4	6488 ± 213.4	3133.3 ± 4.46	3186 ± 69.3
a1	0.895	0.534	0.955	0.392
Rt	36.66 ± 13.1	42.21 ± 0.46	62.70 ± 14.31	96.24 ± 71.24
Qf (µS*sâ)	3868 ± 151.8	1406 ± 24.69	440.4 ± 21.7	752.6 ± 0.04
a2	0.5788	0.832	0.516	0.765
Rf (Ω)	523.0 ± 22.08	1034 ± 51.18	1929 ± 68.38	1369 ± 124.9
X^2 Chi square	3.59 e^{-3}	5.16 e^{-3}	2.78 e^{-3}	6.53 e^{-3}

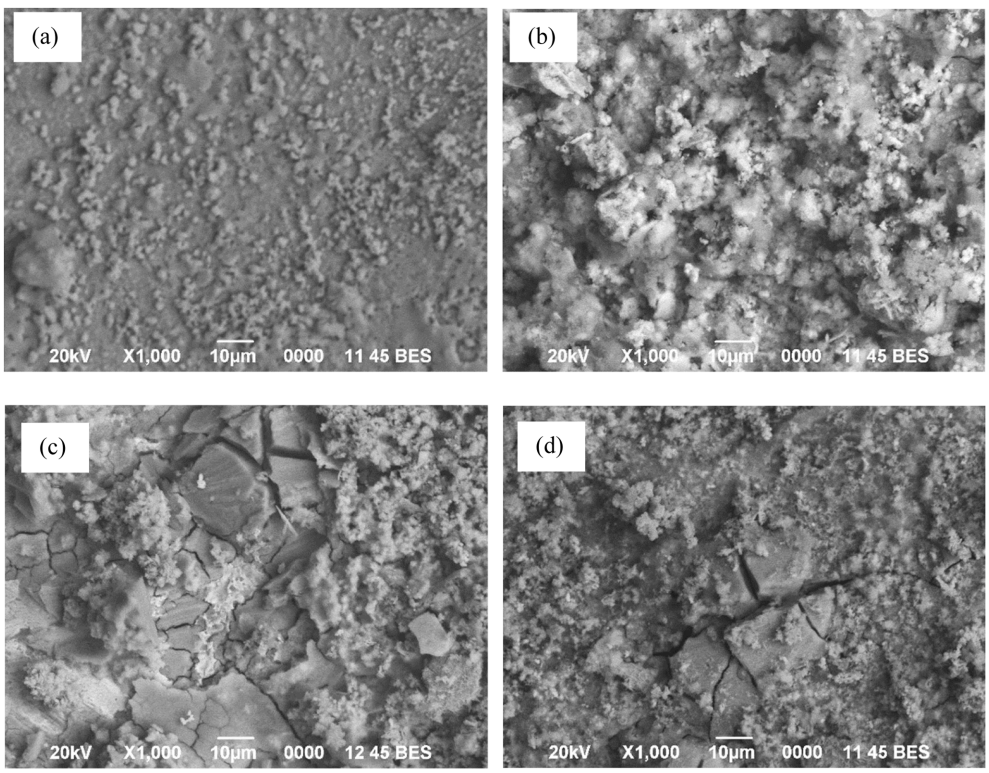

Fig. 6. Surface Morphology After Polarization of (a) without Ni addition, (b) 1 wt%, (c) 2 wt% Ni and (d) 3 wt% Ni

content, the impedance at high frequency appears to increase, close to 5-8.736 Ω (Rs), implying the rate of oxygen reduction accelerated, further slowing corrosion rate [28]. Referring to the findings, adding nickel lowered the corrosion reaction associated with the bainite phase.

The morphologies of surface corrosion after wet/dry cyclic corrosion and polarization test are shown in Fig. 6. Fig. 6a depicts a corrosion surface with tiny granules and without cracks. There are evident cracks in the dense corrosion product by increasing nickel content (Fig. 6c-d). The cracks facilitate the electrolyte to penetrate into metal surface, inducing corrosion may occur quickly due to the presence of active phases [23].

4. Conclusions

The inverted austempering multi-step (IAM) successfully generated a refined bainite structure,

resulting in improved mechanical characteristics and corrosion resistance of Fe-Ni steel. With the nickel addition, the IAM process produced high strength (ultimate strength ~1480 MPa and yield strength ~684 MPa) without significant loss of ductility (~15%) by avoiding blocky austenite and shortening the process time. In the same of heat treatment process, the addition of nickel to Fe-Ni bainitic steel reduced the lath bainite to 4.67 μm, increased the bainite volume fraction to 40.98%, and refined the martensite/austenite grain size to 1.34 μm as a result of the shifted ferrite - austenite transformation and provided more austenite for bainitic transformation, obtaining the higher strength indirectly. Furthermore, nickel contributed to strengthen grain refinement in Fe-Ni steel. In a 3.5 vol.% NaCl solution, Fe-Ni bainitic steel with IAM process shows the higher corrosion resistance than steel processed by single austempering. A higher fraction of bainite phase in Fe-Ni steel resulted in lower corrosion rate ~0.02 mm/year, more positive corrosion potential ~578.8 mV and smaller current corrosion ~0.062 μA/cm^2 due to the generating of more stable oxide layer with crack by adding nickel.

Acknowledgments

All authors thank to Research Center for Metallurgy – BRIN for Funding supports and laboratory facilities

References

1. P. Lambert, Sustainability of metals and alloys in construction, in *Sustainability of Construction Materials*, *2nd ed.,* pp. 105 – 128, Elsevier Ltd (2016).
2. J. Jia, Z. Liu, X. Cheng, C. Du, and X. Li, Development and optimization of Ni-advanced weathering steel: A review, *Corrosion Communication*, **2**, 82 (2021). Doi: https://doi.org/10.1016/j.corcom.2021.09.003
3. W. Wu, X. Cheng, J. Zhao, and X. Li, Benefit of the corrosion product film formed on a new weathering steel containing 3% nickel under marine atmosphere in Maldives, *Corrosion Science*, **165**, 108416 (2020). Doi: https://doi.org/10.1016/j.corsci.2019.108416
4. X. Cheng, Z. Jin, M. Liu, and X. Li, Optimizing the nickel content in weathering steels to enhance their corrosion resistance in acidic atmospheres, *Corrosion Science*, **115**, 135 (2017). Doi: https://doi.org/10.1016/j.corsci.2016.11.016
5. M. Morcillo, I. Díaz, H. Cano, B. Chico, and D. de la Fuente, Atmospheric corrosion of weathering steels. Overview for engineers. Part I: Basic concepts, *Construction and Building Materials*, **213**, 723 (2019). Doi: https://doi.org/10.1016/j.conbuildmat.2019.03.334
6. J. Cheng, J. Qing, Y. Guo, and H. Shen, High-strength weathering steels obtained using bainite matrix and nanoscale co-precipitation, *Materials Letters*, **236**, 307 (2019). Doi: https://doi.org/10.1016/j.matlet.2018.10.076
7. T. Zhang, W. Liu, L. Chen, B. Dong, W. Yang, Y. Fan, Y. Zhao, On how the corrosion behavior and the functions of Cu, Ni and Mo of the weathering steel in environments with different NaCl concentrations, *Corrosion Science*, **192**, 109851 (2021). Doi: https://doi.org/10.1016/j.corsci.2021.109851
8. Neetu, P. K. Katiyar, S. Sangal, and K. Mondal, Effect of various phase fraction of bainite, intercritical ferrite, retained austenite and pearlite on the corrosion behavior of multiphase steels, *Corrosion Science*, **178**, 109043 (2021). Doi: https://doi.org/10.1016/j.corsci.2020.109043
9. X. M. Xiao, Y. Peng, C. Y. Ma, and Z. L. Tian, Effects of Alloy Element and Microstructure on Corrosion Resistant Property of Deposited Metals of Weathering Steel, *Journal of Iron and Steel Research International*, **23**, 171 (2016). Doi: https://doi.org/10.1016/S1006-706X(16)30030-9
10. ASTM A588/A588M-01, Standard Specification for High-Strength Low-Alloy Structural Steel with 50 ksi [345 MPa] Minimum Yield Point to 4 in. [100 mm] Thick[1], ASTM International (2001).
11. H. Mousalou, S. Yazdani, B. Avishan, N. P. Ahmadi, A. Chabok, and Y. Pei, Microstructural and mechanical properties of low-carbon ultra-fine bainitic steel produced by multi-step austempering process, *Materials Science and Engineering: A*, **734**, 329 (2018). Doi: https://doi.org/10.1016/j.msea.2018.08.008
12. G. Gao, H. Guo, X. Gui, Z. Tan, and B. Bai, Inverted multi-step bainitic austempering process routes: Enhanced strength and ductility, *Materials Science and Engineering: A*, **736**, 298 (2018). Doi: https://doi.org/10.1016/j.msea.2018.08.091
13. Z. Yao, G. Xu, H. Hu, Q. Yuan, J. Tian, and M. Zhou, Effect of Ni and Cr Addition on Transformation and Properties of Low-Carbon Bainitic Steels, *Transcations of the Indian Institute of Metals*, **72**, 1167 (2019). Doi: https://doi.org/10.1007/s12666-019-01590-7
14. B. Adamczyk-Cieślak, M. Koralnik, R. Kuziak, K.

Majchrowicz, T. Zygmunt, and J. Mizera, The Impact of Retained Austenite on the Mechanical Properties of Bainitic and Dual Phase Steels, *Journal of Materials Engineering and Performance*, **31**, 4419 (2022). Doi: https://doi.org/10.1007/s11665-021-06547-w

15. H. Y. Dong, C. Y. Hu, G. H. Wu, K. M. Wu, and R. D. K. Misra, A Effect of nickel on hardening behavior and mechanical properties of nanostructured bainite-austenite steels, *Materials Sciences and Engineering: A,* **817**, 141410 (2021). Doi: https://doi.org/10.1016/j.msea.2021.141410
16. J. Tian, G. Xu, Z. Jiang, H. Hu, and M. Zhou, Effect of Ni Addition on Bainite Transformation and Properties in a 2000 MPa Grade Ultrahigh Strength Bainitic Steel, *Metals and Materials International*, **24**, 1202 (2018). Doi: https://doi.org/10.1007/s12540-018-0139-y
17. S. Chen, J. Hu, L. Shan, C. Wang, X. Zhao, and W. Xu, Characteristics of bainitic transformation and its effects on the mechanical properties in quenching and partitioning steels, *Materials Science and Enginnering: A*, **803**, 140706 (2021). Doi: https://doi.org/10.1016/j.msea.2020.140706
18. F. Citrawati, R. Dwiwandono, and L. Firmansyah, The effect of Ni on the formation of bainite in Fe-Ni lateritic steels through semi-continuous cooling method, *International Journal of Technology*, **11**, 60 (2020). Doi: https://doi.org/10.14716/ijtech.v11i1.3178
19. M. Arribas, T. Gutiérrez, E. D. Molino, A. Arlazarov, I. D. D.-C., D. Martin, D. D. Caro, S. Ayenampudi, and M. J. Santofimia, Austenite reverse transformation in a Q&P route of Mn and Ni added steels, *Metals,* **10**, 862 (2020). Doi: https://doi.org/10.3390/met10070862
20. A. P. Moon, K. Chandra Sekhar, S. Mahanty, S. Sangal, and K. Mondal, Corrosion Behavior of Newly Developed High-Strength Bainitic Railway Wheel Steels, *Journal of Materials Engineering and Performance*, **29**, 3443 (2020). Doi: https://doi.org/10.1007/s11665-020-04846-2
21. T. Rojhirunsakool, T. Thublaor, M. H. S. Bidabadi, S. Chandra-Ambhorn, Z. Yang, and G. Gao, Corrosion Behavior of Multiphase Bainitic Rail Steels, *Metals*, **12**, 694 (2022). Doi: https://doi.org/10.3390/met12040694
22. A. Yilmaz, X. Li, S. Pletincx, T. Hauffman, J. Sietsma, and Y. Gonzalez-Garcia, Passive Film Properties of Martensitic Steels in Alkaline Environment: Influence of the Prior Austenite Grain Size, *Metals ,* **12**, 292 (2022). Doi: https://doi.org/10.3390/met12020292
23. Neetu, P. K. Katiyar, S. Sangal, and K. Mondal, Effect of various phase fraction of bainite, intercritical ferrite, retained austenite and pearlite on the corrosion behavior of multiphase steels, *Corrosion Science*, **178**, 109043 (2021). Doi: https://doi.org/10.1016/j.corsci.2020.109043
24. C. Thee, L. Hao, J. H. Dong, X. Mu, and W. Ke, Numerical approach for atmospheric corrosion monitoring based on EIS of a weathering steel, *Acta Metallurgica Sinica (English Letters)*, **28**, 261 (2015). Doi: https://doi.org/10.1007/s40195-014-0193-5